





Article

Design, Synthesis and Biological Evaluation of 1,3,5-Triazine Derivatives Targeting hA₁ and hA₃ Adenosine Receptor

Sujin Park ^{1,2}, Yujin Ahn ^{3,4} , Yongchan Kim ², Eun Joo Roh ², Yoonji Lee ⁵ , Chaebin Han ^{1,2}, Hee Min Yoo ^{3,4,*}  and Jinha Yu ^{1,*} 

- ¹ College of Pharmacy and Graduate School of Pharmaceutical Sciences, Ewha Womans University, Seoul 03760, Korea; sujinp@kist.re.kr (S.P.); 121521@kist.re.kr (C.H.)
² Biomedical Research Institute, Korea Institute of Science and Technology (KIST), Seoul 02792, Korea; riskywing@gmail.com (Y.K.); r8636@kist.re.kr (E.J.R.)
³ Biometrology Group, Korea Research Institute of Standards and Science (KRIS), Daejeon 34113, Korea; yujinahn2202@gmail.com
⁴ Department of Precision Measurement, University of Science and Technology (UST), Daejeon 34113, Korea
⁵ College of Pharmacy, Chung-Ang University, Seoul 06974, Korea; yoonjilee@cau.ac.kr
 * Correspondence: hmy@kriss.re.kr (H.M.Y.); jhyu@ewha.ac.kr (J.Y.)

Abstract: Adenosine mediates various physiological activities in the body. Adenosine receptors (ARs) are widely expressed in tumors and the tumor microenvironment (TME), and they induce tumor proliferation and suppress immune cell function. There are four types of human adenosine receptor (hARs): hA₁, hA_{2A}, hA_{2B}, and hA₃. Both hA₁ and hA₃ AR play an important role in tumor proliferation. We designed and synthesized novel 1,3,5-triazine derivatives through amination and Suzuki coupling, and evaluated them for binding affinities to each hAR subtype. Compounds **9a** and **11b** showed good binding affinity to both hA₁ and hA₃ AR, while **9c** showed the highest binding affinity to hA₁ AR. In this study, we discovered that **9c** inhibits cell viability, leading to cell death in lung cancer cell lines. Flow cytometry analysis revealed that **9c** caused an increase in intracellular reactive oxygen species (ROS) and a depolarization of the mitochondrial membrane potential. The binding mode of 1,3,5-triazine derivatives to hA₁ and hA₃ AR were predicted by a molecular docking study.

Keywords: adenosine receptor; dual ligand; 1,3,5-triazine; molecular docking; antitumor agents



Citation: Park, S.; Ahn, Y.; Kim, Y.; Roh, E.J.; Lee, Y.; Han, C.; Yoo, H.M.; Yu, J. Design, Synthesis and Biological Evaluation of 1,3,5-Triazine Derivatives Targeting hA₁ and hA₃ Adenosine Receptor. *Molecules* **2022**, *27*, 4016. <https://doi.org/10.3390/molecules27134016>

Academic Editor: Loredana Cappellacci

Received: 13 May 2022

Accepted: 20 June 2022

Published: 22 June 2022

Publisher's Note: MDPI stays neutral with regard to jurisdictional claims in published maps and institutional affiliations.



Copyright: © 2022 by the authors. Licensee MDPI, Basel, Switzerland. This article is an open access article distributed under the terms and conditions of the Creative Commons Attribution (CC BY) license (<https://creativecommons.org/licenses/by/4.0/>).

1. Introduction

Extracellular adenosines are important signal transmitters and mediate various physiological activities in the body [1,2]. Human adenosine receptors (hARs) can be classified into four subtypes: hA₁, hA_{2A}, hA_{2B}, and hA₃. All four belong to the G protein-coupled receptor (GPCR) family, and each has a different pharmacological profile, tissue distribution, and function [3]. Although hARs have been known for a long time, new functions are continuously being discovered and novel ligands being developed.

hA₁ AR is found in various tissues and cells and regulates many physiological activities in the body; for example, the activation of hA₁ AR leads to bradycardia [4], inhibits neurotransmitter release [5], lipolysis [6], and renal excretion [7] and induces smooth muscle contraction [8]. The hA₁ AR agonist has mainly been developed for treatment of cardiovascular diseases, such as heart failure, arrhythmia, and angina, or for neurological diseases, such as seizure, ischemia, and depression [9].

hA₃ AR is also important for physiological signaling in the body. hA₃ AR is expressed at a low level in most cells but is overexpressed in inflammatory and various neoplastic cells [10]. Therefore, it is an important drug target for developing therapeutic agents for glaucoma, stroke, asthma, inflammation, rheumatoid arthritis, and cancer [11].

Multiple studies have demonstrated that hA₁ AR regulates the proliferation of tumor cells and that hA₁ AR antagonists inhibit the proliferation and migration of tumor cells [12]. It is unclear exactly what function hA₃ AR has in tumor cell proliferation and death [13,14]. Numerous publications have shown that hA₃ AR is overexpressed in various types of cancer cells [15]. The activation of hA₃ AR induces the growth of tumor cells by increasing VEGF, HIF-1, MMP-9, angiogenesis, migration, and proliferation [16]. At the same time, it decreases cell proliferation by induction of G-CSF and IL-2 in the immune system [17].

Polypharmacology, a concept that controls multiple targets with one drug, is a new paradigm in drug discovery that has recently received attention [18]. Compared with combination therapy, polypharmacology has higher safety and lower risk of drug–drug interaction [19]. hA₁ and hA₃ AR are good targets for multitarget drugs because among hARs, hA₁ and hA₃ AR are quite similar, with 49% sequence similarity [3]. In addition, the two are activated by the same endogenous ligand, adenosine, and the downstream signal also inhibits cyclic adenosine monophosphate (cAMP) production in the same way.

Determining what alterations tumor cells undergo when simultaneously inhibiting both hA₁ and hA₃ AR that share a sub-signal transduction will be an important step in the development of anticancer drugs targeting adenosine receptors. Several studies on ligands that simultaneously regulate hA₁ and hA₃ AR have been published [20–22]. Compound 1 bearing a purine scaffold shows an inhibition constant (K_i) of 6.8 and 6.3 nM, and compound 2 shows a K_i of 36.7 and 25.4 nM for hA₁ and hA₃ AR, respectively, indicating balanced binding (Figure 1).

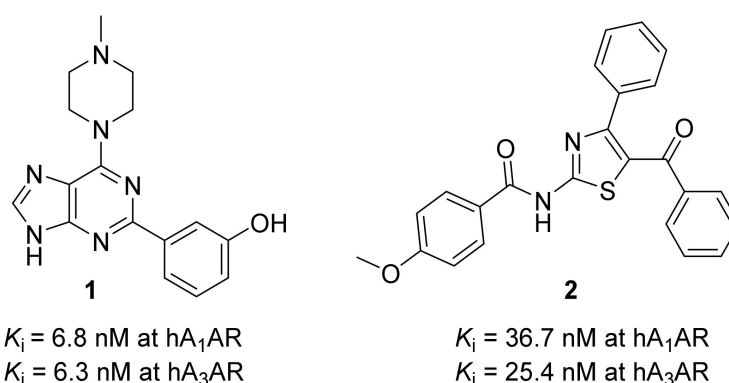


Figure 1. The structure of dual hA₁–hA₃ AR antagonists. AR: adenosine receptor.

To develop a novel scaffold of the hAR ligand in non-xanthine ligands, we analyzed previously reported compounds targeting adenosine receptors. Langmead et al., in an effort to find a novel hit through a docking study, reported that compounds containing 1,3,5-triazine bind to hA₁ and hA_{2A} AR (Figure 2) [23]. Compound 3 was found to be an hA_{2A} AR antagonist, with moderate selectivity (9.5-fold) against hA₁ AR. Compound 4 was discovered through virtual screening and bound more potently compared to compound 3, but the selectivity against hA₁ AR was 2.94, which was lower compared to compound 3 [24].

Compound 5 (1,3,5-triazine-thiadiazole) has been described as a potent hA_{2A} AR antagonist [25,26]. Compound 6 showed 319-fold selectivity against hA_{2A} AR compared to hA₁ AR; however, the selectivity index (hA₁ AR:hA_{2A} AR) of compound 5 was 11.66, indicating low selectivity. On the basis of previously published research, it was determined that derivatives of the 1,3,5-triazine scaffold were ligands that modulate adenosine receptors. In addition, the type of triazine substituents altered the subtype selectivity of adenosine receptors. This indicates that triazine modifications could be optimized to produce selective ligands for subtypes other than hA_{2A} AR. Therefore, we attempted to introduce various substitutions into 1,3,5-triazine in order to provide specific ligands for hA₁ and hA₃ AR.

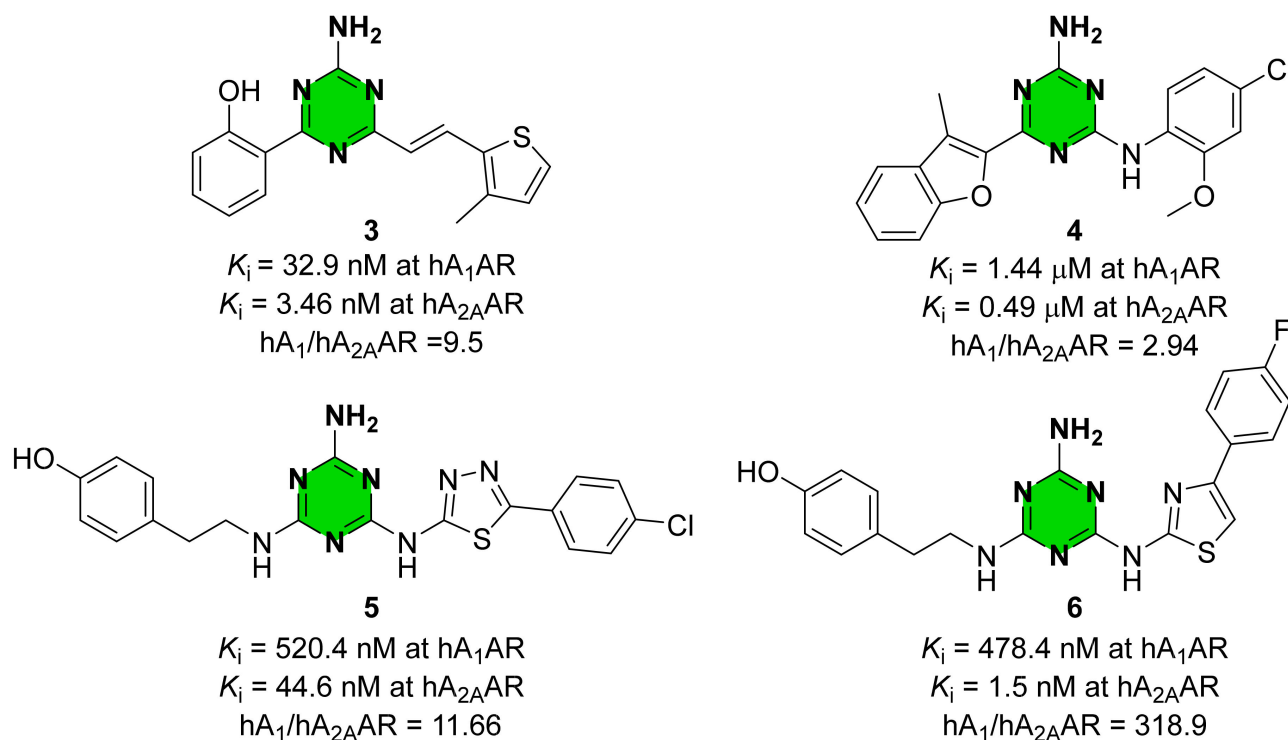


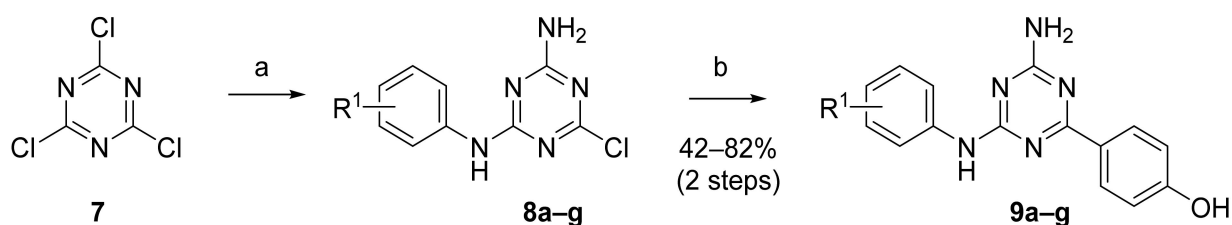
Figure 2. 1,3,5-Triazine derivatives as hAR ligands. AR: adenosine receptor.

In this study, we developed a series of 1,3,5-triazine derivatives that bind to hA_1 and hA_3 AR by substituting at the 2, 4, and 6 positions of the 1,3,5-triazine scaffold. A novel 2-amino-1,3,5-triazine derivative was designed by introducing substituents at the 4 and 6 positions of 1,3,5-triazine. The designed derivatives were synthesized, and their binding affinities to hARs were evaluated using a radioligand. The binding mode of 1,3,5-triazine derivatives were predicted by a molecular docking study using the crystal structure of the hA_1 AR (PDB ID: 5N2S) and a homology model of the hA_3 AR [27].

2. Results and Discussion

2.1. Synthesis of 1,3,5-Triazine Derivatives

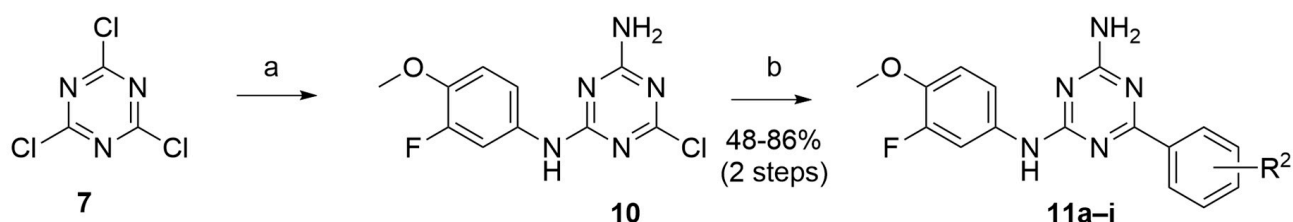
2-Amino-1,3,5-triazine derivatives were prepared as described in Scheme 1. Briefly, cyanuric chloride (**7**) was reacted with various types of anilines to obtain **8a–g**, followed by amination using aqueous ammonia (25–28% in water), synthesizing **9a–g**. Suzuki coupling with (4-hydroxyphenyl) boronic acid and **8a–g** in the presence of $\text{Pd}(\text{PPh}_3)_4$ yielded **9a–g** in moderate-to-good yield (42–82%).



Reagents and conditions: a) i) various anilines, THF, $-15 \text{ }^\circ\text{C}$, 30 min; ii) NH_4OH in water (25%–28%), rt, 2 h; b) (4-OHPh)B(OH)₂, $\text{Pd}(\text{PPh}_3)_4$, K_2CO_3 , 1,4-dioxane, water, $90 \text{ }^\circ\text{C}$, 16 h or μW , $120 \text{ }^\circ\text{C}$, 50 min.

Scheme 1. Synthesis of 2-(4-hydroxyphenyl)-4-amino-1,3,5-triazine derivatives. THF: tetrahydrofuran.

Based on compound **8a**, we synthesized derivatives including 3-fluoro-4-methoxyaniline at the 4 position of 1,3,5-triazine through amination and Suzuki coupling (Scheme 2). Stepwise amination of cyanuric chloride using 3-fluoro-4-methoxyaniline and ammonium hydroxide yielded **10**, and Suzuki coupling with **10** and various boronic acids yielded the condensed compounds (**11a–i**).



Reagents and conditions: a) i) 3-fluoro-4-methoxyaniline, THF, $-15\text{ }^\circ\text{C}$, 30 min; ii) NH_4OH in water (25%–28%), rt, 2 h; b) $R^2PhB(OH)_2$, $Pd(PPh_3)_4$, K_2CO_3 , 1,4-dioxane, water, $90\text{ }^\circ\text{C}$, 16 h or μW , $120\text{ }^\circ\text{C}$, 50 min.

Scheme 2. Synthesis of 6-(3-fluoro-4-methoxyaniline)-4-amino-1,3,5-triazine derivatives. THF: tetrahydrofuran.

2.2. Radioligand Binding Assays at Human Adenosine Receptors

All the synthesized compounds were screened with radioligand binding assays at hARs [28]. First, the percentage of inhibition was measured by treatment of each hAR subtype with $10\text{ }\mu\text{M}$ of each compound (Table 1). Except for **9c**, all compounds showed $<90\%$ inhibition at hA_{2A} and hA_{2B} AR. Compounds **9a–c**, **9e**, and **9g** showed $>95\%$ inhibition at hA_1 AR, and compounds **9a**, **9c**, and **9d** showed $>95\%$ inhibition at hA_3 AR. In addition, **9d** showed 69% inhibition at hA_1 AR whereas it showed 95% inhibition at hA_3 AR, showing significant selectivity. Compound **9c** showed $>95\%$ inhibition at all subtypes except hA_{2B} AR. Compound **9f** including 4-*N*-piperidine showed no binding with any of the subtypes, probably because the large piperidine interfered with binding to the hARs.

The binding affinities of compounds showing $>95\%$ inhibition were determined and are shown in Table 2. Compound **9a** with 3-fluoro-4-methoxyaniline showed the best binding affinity to hA_3 AR ($K_i = 55.5\text{ nM}$) and good binding affinity to hA_1 AR, with a 2.5-fold hA_1 AR: hA_3 AR selectivity index. Compound **9b** with 3,5-dimethoxyaniline also showed potent and selective binding affinity to hA_1 AR ($K_i = 69.7\text{ nM}$). Compound **9c** with 3-methoxy-4-chloroaniline showed the best binding affinity to hA_1 AR ($K_i = 57.9\text{ nM}$) and moderate binding affinity to hA_3 AR ($K_i = 661.1\text{ nM}$). R^1 substitution in the aniline appeared to be well tolerated by hA_1 AR compared to hA_3 AR. The compounds substituted with methoxy in aniline generally showed good binding affinity to hA_1 AR, with higher affinity being obtained with compounds bearing meta-methoxy attached to the aniline core. Moreover, the compounds with methoxy substituted at the *para*-position of aniline showed the best binding affinity.

Since the most balanced binding to hA_1 AR: hA_3 AR was shown by **9a**, we developed a series of 3-fluoro-4-methoxyaniline derivatives **11a–i** for dual hA_1 – hA_3 AR ligands. Various substituents were introduced at the *para*-position of phenyl to replace the hydroxyl group, and the percentage inhibition was evaluated at the four hAR subtypes with $10\text{ }\mu\text{M}$ of the synthesized compounds (Table 3). Compounds **11a** and **11b**, which included methoxy and fluorine at the *para*-position of benzene, respectively, displayed $>90\%$ inhibition at both hA_1 and hA_3 AR and low percentage inhibition at hA_{2A} and hA_{2B} AR. Compounds **11c–e** substituted with the electron-withdrawing groups OCF_3 , CF_3 , and CN , respectively, at the *para*-position of the phenyl core showed low percentage inhibition at all hAR subtypes. The compounds bearing a bulky group attached to the *para*-position of the phenyl core also showed low percentage inhibition at all hARs, indicating that the substituent at the *para*-position of the phenyl core is likely to be important for determining the binding affinity at hARs. Compounds **11h** and **11i** bearing two fluorine and nitro at the meta-position of the phenyl core, respectively, showed much lower percentage inhibition compared to **9a** and

11b. We deduce that substituents at a position other than the *para*-position of the phenyl core negatively affect binding to hARs.

Table 1. Percentage inhibition of 2-(*p*-phenol)-4-amino-1,3,5-triazine derivatives **9a–g** at hA₁, hA_{2A}, hA_{2B}, and hA₃ ARs.

9a–g

Compound	R ¹	Percentage Inhibition (%) at 10 μM ^a			
		hA ₁ AR	hA _{2A} AR	hA _{2B} AR	hA ₃ AR
9a	3-F-4-OCH ₃	99 ± 1	58 ± 1	72 ± 2	97 ± 1
9b	3,5-(OCH ₃) ₂	99 ± 1	84 ± 4	62 ± 2	93 ± 1
9c	3-OCH ₃ -4-Cl	99 ± 1	94 ± 3	90 ± 1	95 ± 1
9d	3-CF ₃	69 ± 2	40 ± 5	74 ± 1	95 ± 1
9e	3,5-(CH ₃) ₂	96 ± 3	58 ± 3	42 ± 2	92 ± 1
9f	4- <i>N</i> -piperidine	28 ± 1	28 ± 3	44 ± 4	38 ± 1
9g	2,4-(CH ₃) ₂	99 ± 1	80 ± 4	47 ± 2	91 ± 1

^a All binding experiments were performed using adherent mammalian cells stably transfected with cDNA encoding the appropriate hAR (hA₁ and hA₃ AR in CHO cells, hA_{2A} AR in HeLa cells, and hA_{2B} AR in HEK-293 cells). Binding was carried out using 2 nM [³H]DPCPX, 3 nM [³H]ZM241385, 25 nM [³H]DPCPX, and 0.5 nM [³H]NECA as radioligands for hA₁, hA_{2A}, hA_{2B}, and hA₃ AR, respectively. Values are expressed as the percentage inhibition of specific radioligand binding at 10 μM, with nonspecific binding defined using 10 μM NECA. AR: adenosine receptor; cDNA: complementary DNA; CHO: Chinese hamster ovary; DPCPX: 8-cyclopentyl-1,3-dipropylxanthine; hAR: human adenosine receptor; HEK: human embryonic kidney; NECA: 5-*N*-ethylcarboxamido adenosine.

Table 2. Binding affinity to hA₁ and hA₃ ARs.

Compound	R ¹	K _i (nM) ^a		Selectivity (hA ₁ AR:hA ₃ AR)
		hA ₁ AR	hA ₃ AR	
9a	3-F-4-OCH ₃	139.3	55.5	2.51
9b	3,5-(OCH ₃) ₂	69.7	ND	-
9c	3-OCH ₃ -4-Cl	57.9	661.1	0.0875
9d	3-CF ₃	ND	1258	-
9e	3,5-(CH ₃) ₂	872.1	ND	-
9f	4- <i>N</i> -piperidine	ND	ND	-
9g	2,4-(CH ₃) ₂	116.5	ND	-

^a All binding experiments were performed using adherent mammalian cells stably transfected with cDNA encoding the appropriate hAR (hA₁ and hA₃ in CHO cells). Binding was carried out using 2 nM [³H]DPCPX and 0.5 nM [³H]NECA as radioligands for hA₁ and hA₃ AR, respectively. AR: adenosine receptor; cDNA: complementary DNA; CHO: Chinese hamster ovary; DPCPX: 8-cyclopentyl-1,3-dipropylxanthine; hAR: human adenosine receptor; ND: not determined; NECA: 5-*N*-ethylcarboxamido adenosine.

The binding affinities of **11a** and **11b** at hA₁ and hA₃ AR were determined and are shown in Table 4. Compound **11a** with methoxy instead of a hydroxyl group showed improved binding affinity to both hA₁ and hA₃ AR, about 2-fold at hA₁ AR and 5-fold at hA₃ AR, with an hA₁ AR:hA₃ AR selectivity index of 5.87. For **11b** bearing *para*-fluorine at the phenyl core, the binding affinity was less changed; however, the binding affinity to hA₁ AR slightly improved, indicating an hA₁ AR:hA₃ AR selectivity index of 1.7.

Table 3. Percentage inhibition of 6-(3-fluoro-4-methoxyaniline)-4-amino-1,3,5-triazine derivatives **11a–i** at hA₁, hA_{2A}, hA_{2B}, and hA₃ ARs.

11a-i

Compound	R ²	Percentage Inhibition (%) at 10 μM ^a			
		hA ₁ AR	hA _{2A} AR	hA _{2B} AR	hA ₃ AR
9a	4-OH	99 ± 1	56 ± 3	66 ± 3	97 ± 1
11a	4-OCH ₃	95 ± 1	83 ± 1	65 ± 2	97 ± 1
11b	4-F	98 ± 1	49 ± 1	56 ± 1	95 ± 4
11c	4-OCF ₃	48 ± 4	81 ± 1	27 ± 6	60 ± 1
11d	4-CF ₃	74 ± 1	30 ± 1	93 ± 3	79 ± 1
11e	4-CN	45 ± 5	50 ± 2	52 ± 1	72 ± 3
11f	4-C(O)OCH ₃	52 ± 1	35 ± 6	55 ± 2	85 ± 1
11g	4-C(O)OCH ₂ CH ₃	56 ± 1	48 ± 6	35 ± 2	78 ± 3
11h	3,5-diF-4-OH	88 ± 1	26 ± 5	66 ± 6	79 ± 1
11i	3-NO ₂ -4-F	53 ± 1	57 ± 2	72 ± 6	83 ± 1

^a All binding experiments were performed using adherent mammalian cells stably transfected with cDNA encoding the appropriate hAR (hA₁ and hA₃ in CHO cells, hA_{2A} in HeLa cells, and hA_{2B} in HEK-293 cells). Binding was carried out using 2 nM [³H]DPCPX, 3 nM [³H]ZM241385, 25 nM [³H]DPCPX, and 0.5 nM [³H]NECA as radioligands for hA₁, hA_{2A}, hA_{2B}, and hA₃ AR, respectively. Values are expressed as the percentage inhibition of a specific radioligand binding at 10 μM, with nonspecific binding defined using 10 μM NECA. AR: adenosine receptor; cDNA: complementary DNA; CHO: Chinese hamster ovary; DPCPX: 8-cyclopentyl-1,3-dipropylxanthine; hAR: human adenosine receptor; HEK: human embryonic kidney; NECA: 5-*N*-ethylcarboxamido adenosine.

Table 4. Binding affinity to hA₁ and hA₃ ARs.

Compound	R ²	K _i (nM) ^a		Selectivity (hA ₁ AR:hA ₃ AR)
		hA ₁ AR	hA ₃ AR	
9a	4-OH	139.3	55.5	2.51
11a	4-OCH ₃	78.1	13.3	5.87
11b	4-F	98.3	56.6	1.74

^a All binding experiments were performed using adherent mammalian cells stably transfected with cDNA encoding the appropriate hAR (hA₁ and hA₃ in CHO cells). Binding was carried out using 2 nM [³H]DPCPX and 0.5 nM [³H]NECA as radioligands for hA₁ and hA₃ AR, respectively. AR: adenosine receptor; cDNA: complementary DNA; CHO: Chinese hamster ovary; DPCPX: 8-cyclopentyl-1,3-dipropylxanthine; hAR: human adenosine receptor; NECA: 5-*N*-ethylcarboxamido adenosine.

2.3. cAMP Assay at hA₁ and hA₃ AR Adenosine Receptors

To determine whether 1,3,5-triazine scaffold derivatives behave as agonists or antagonists, we performed cAMP accumulation assays with **11a** and **11b** at hA₁ and hA₃ AR. We confirmed whether the test compounds behave as antagonists by measuring the concentration change in cAMP in the presence of a full agonist 5-*N*-ethylcarboxamido adenosine (NECA) using antagonist mode assays. We also confirmed whether the test compounds could behave as agonists by comparing the relative percentage activation of NECA using agonist mode assays. Both **11a** and **11b** showed 77% and 88% inhibition at hA₃ AR in antagonist mode, respectively, and 17% and 6% percentage activation in agonist mode, respectively, indicating that **11a** and **11b** behave as antagonists at hA₃ AR.

Compound **11b** showed 60% inhibition in antagonist mode and 23% activation in agonist mode, confirming that it acts as an antagonist and a partial agonist for hA₁ AR. However, the assay results of **11a** at hA₁ AR were interesting. The percentage inhibition and percentage activation of **11a** were 1% and 11% in antagonist mode and agonist mode, respectively, indicating that **11a** is neither an antagonist nor an agonist for hA₁ AR. That is, **11a** binds to hA₁ AR with high binding affinity, and the cAMP concentration does not change due to **11a** binding. Thus, additional experiments are required to determine which signaling transduction occurs after **11a** binds to hA₁ AR.

2.4. Cell Viability of 1,3,5-Triazine Derivatives **9a–c**, **9g**, and **11a–b**

To test the effect of the compounds in terms of cell growth regulation in lung cancer cell lines such as A549 and NCI-H1299 cells, these cells were treated in 96-well plates for 48 h with the compounds at concentrations ranging from 0 μ M to 100 μ M. Viability of A549 and NCI-H1299 cells was lowered by treatment with 1,3,5-triazine derivatives **9a–c**, **9g**, and **11a–b** which showed good binding affinity at hA₁ AR. However, compound **9a** and **11a–b**, which bound to hA₁ and hA₃ AR, exhibited relatively low cell viability, whereas compound **9c**, which had the highest binding affinity at hA₁ AR among the derivatives, exhibited the greatest inhibitory effect. To assess lung cancer cell viability, a cell viability assay was performed, and the results indicated a significant decrease in cell viability to 59.9% in A549 cells treated with **9c** of 25 μ M concentration, and to 68.8% in NCI-H1299 cells treated with **9c** of 25 μ M concentration (Figure 3A). Therefore, we decided to perform an additional experiment with **9c**. Microscopic analysis of A549 cells treated with 20 μ M and 40 μ M of **9c** further showed that these cells exhibited gradual changes in cell growth in a dose-dependent manner relative to the concentration of **9c** (Figure 3B).

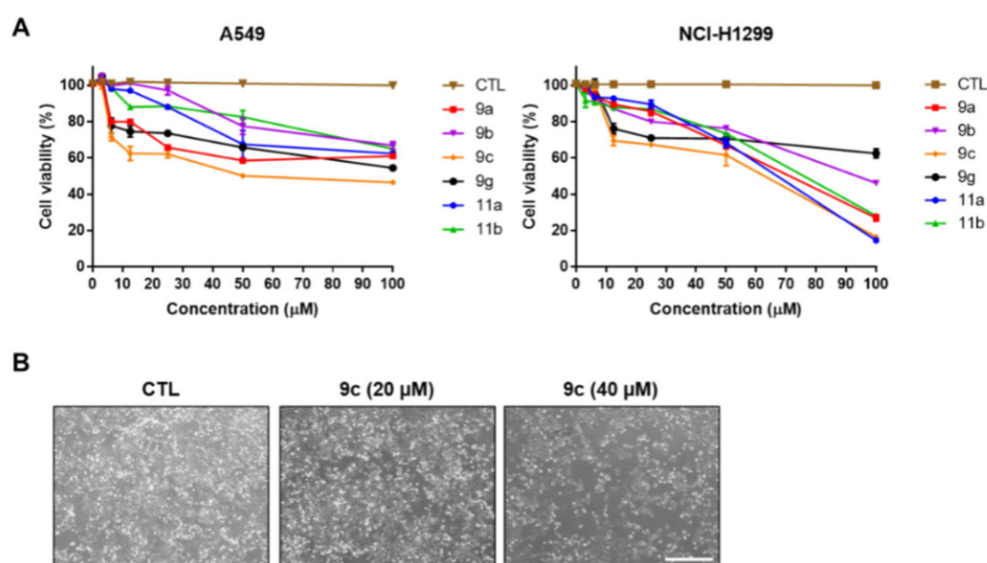


Figure 3. Compound **9c** decreases cell viability in lung cancer cell lines. (A) Cell viability as measured through MTS assays in which A549 and NCI-H1299 cells were exposed to various concentrations of the compounds. (B) Cell morphologies were taken after 48 h of treatment with **9c** (scale bar: 750 μ m).

2.5. Compound **9c**-Induced Intracellular ROS and Mitochondrial ROS

Although reactive oxygen species (ROS) play an important role in regulating normal cellular processes, abnormal ROS levels contribute to the development of a variety of human diseases, including cancer. Because of their accelerated metabolism, cancer cells have higher ROS levels than normal cells [29]. Nevertheless, the high ROS content of cancer cells makes them more susceptible to oxidative stress-induced cell death, which can be used to target cancer cells selectively [30]. Flow cytometry was used to determine whether **9c** induces ROS generation in A549 cells by examining the results. The experiment was

conducted with H₂DCF-DA as a fluorescent probe. As shown in Figure 4A,B, A549 cells treated with **9c** of 20 μ M and 40 μ M concentrations exhibited highly increased ROS of 7.31% and 22.6%, respectively. For comparison, the control sample exhibited a ROS level of 1.26%. Next, we determined the effect of **9c** in regulating mitochondrial ROS. Our results show the **9c**-treated A549 cells to have significantly increased mitochondrial ROS levels (Figure 4C,D). These data indicate that **9c** treatment makes lung cancer cells more sensitive to oxidative stress and makes them more vulnerable to ROS-mediated cell death.

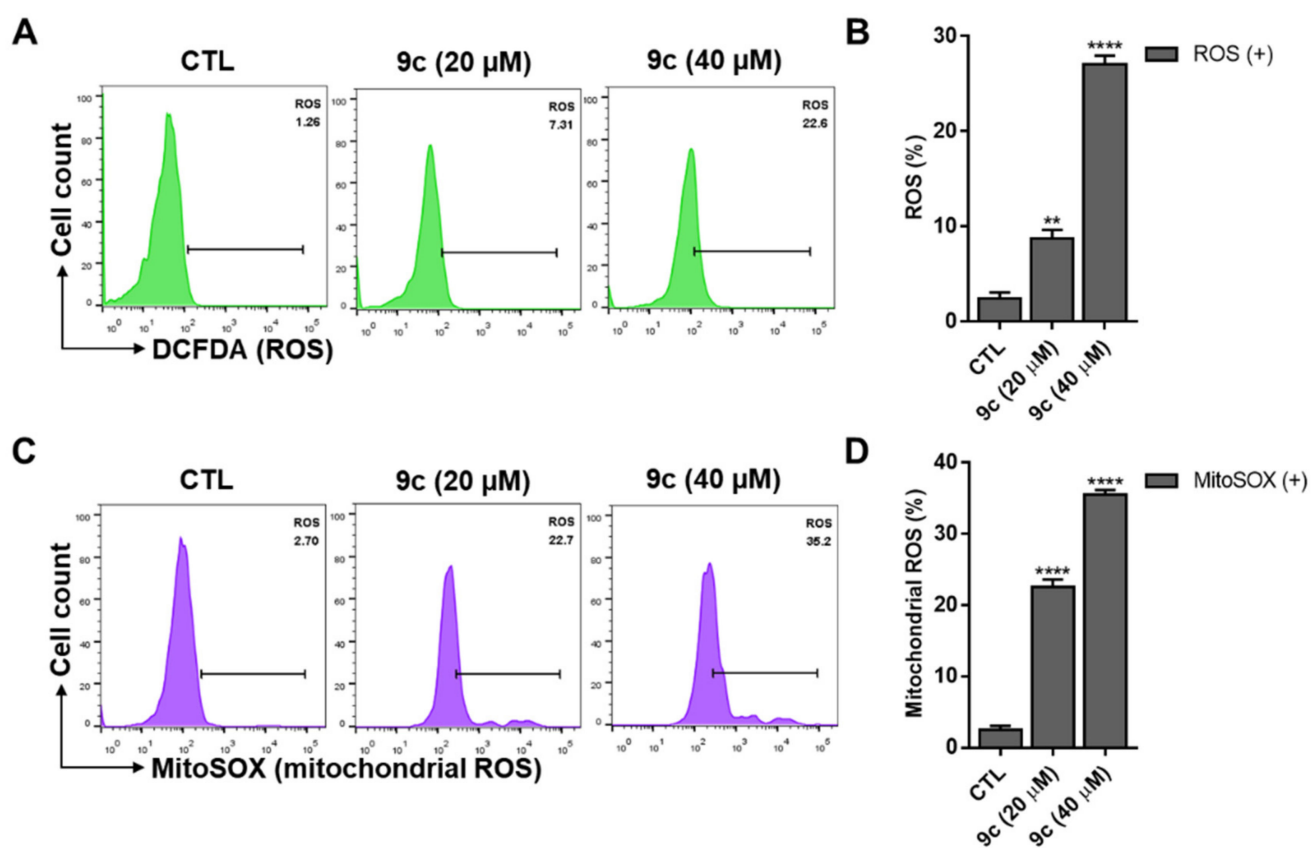


Figure 4. Compound **9c**-induced reactive oxygen species (ROS) generation in A549 cell lines. (A) Changes in ROS levels following treatment with 20 μ M and 40 μ M **9c**, respectively, for 48 h as measured using H₂DCFDA and a flow cytometer. (B) Quantification of ROS levels. (C) A549 cells were treated with **9c** and mitochondrial ROS was indicated by MitoSOX Red. Flow cytometry was employed to analyze the A549 cells. (D) Quantification of mitochondrial ROS levels. Values indicate means \pm SEM. ($n = 3$, ** $p \leq 0.01$, **** $p \leq 0.0001$).

2.6. Compound **9c**-Induced Mitochondrial Membrane Dysfunction

ROS-induced oxidative stress can cause the rapid depolarization of the inner mitochondrial membrane potential ($\Delta\Psi_m$) and, as a result, impairment of oxidative phosphorylation [31]. Using tetramethylrhodamine methyl ester (TMRM) measurements, we investigated how mitochondrial membrane potential was affected by **9c**. A549 cells were exposed to **9c** following incubation with TMRM. Afterward, flow cytometry was employed to calculate the intensity of TMRM binding in the healthy membrane. Figure 5A,B show that, compared to the control value of 93.8%, the TMRM-positive intensity dramatically decreased to 74.6% at 20 μ M, and to 52.3% at 40 μ M, respectively. The results suggest that **9c** causes the A549 cell's mitochondrial membrane to depolarize, which leads to dysfunction.

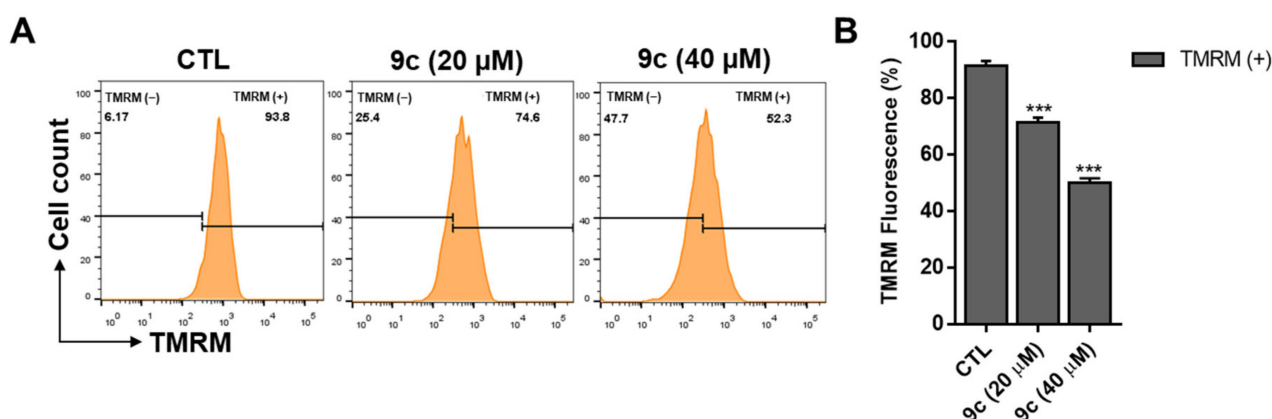


Figure 5. 9c decreases mitochondrial membrane potential in the A549 cell line. (A) Effects of treatment with 20 μM and 40 μM 9c for 48 h on the mitochondrial membrane potential of A549 cells as measured using the TMRM reagent (100 nM) and a flow cytometer. (B) Quantification of mitochondrial membrane potential. Values indicate the means ± SEM. ($n = 3$, *** $p \leq 0.001$).

2.7. Compound 9c Effects on Lung Cancer Cell Death

A live cell assay and a dead cell assay were carried out using a mixture of two fluorescent dyes: calcein (green dye for live cells) and ethidium homodimer-1 (EthD-1, red dye for dead cells). The cells were washed and stained with calcein and EthD-1 before conducting imaging fluorescence microscopy and flow cytometry experiments. When treated with 20 μM 9c, we observed a drastic decrease in the number of live cells (green) and a slight increase in the number of dead cells (red). This was supported by the flow cytometry results, which indicated an approximate increase in the number of dead cells (compared to the control group) by 34.4% following treatment with 20 μM 9c, and by 46.1% following treatment with 40 μM 9c (Figure 6A,B), respectively. As a result, our findings suggest that 9c significantly reduces the viability of lung cancer cell lines.

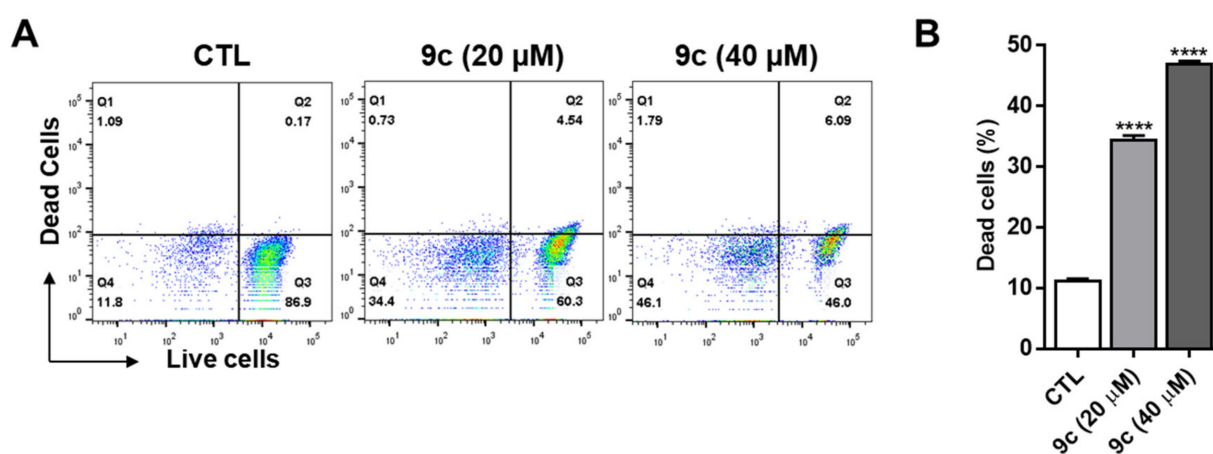


Figure 6. Compound 9c-induced cytotoxic effects on lung cancer cell lines. (A) Live and dead assay performed using a flow cytometer following 9c treatment of A549 cells. (B) Quantification of dead cells. Values indicate means ± SEM. ($n = 3$, *** $p \leq 0.0001$).

2.8. Molecular Docking Study of 1,3,5-Triazine Derivatives

We attempted molecular docking to investigate how the triazine derivatives bind to hA₁ and hA₃ AR. Initially, the binding mode of 11b to hA₁ AR was predicted using x-ray structure (PDB; 5N2S). Consequently, two docking poses of 11b in hA₁ AR were proposed and depicted in Figure 7A. There was no significant difference between the two binding mode docking scores, −9.100 (red) and −8.624 (violet). 11b was stabilized by

π - π interactions between the triazine and F171^{5,29} in the two docking poses. By contrast, N254^{6,5} formed hydrogen bonds with the nitrogen of aniline in the red-binding mode, or nitrogen of amino in the purple-binding mode, respectively. The aniline group of **11b** was oriented toward the augmented TM2 region in hA₁ AR, adopting a purple-binding pose. Docking was also performed on **9a** and **9c**, which both exhibited strong binding affinity in hA₁ AR and were both predicted to bind in the same manner as **11b**. (Supplementary Materials, Figure S3). In addition, **11h** and **11i** with a substituent at the *meta* position of the phenyl ring were also applied to a docking study (Figure 7B). The phenyl rings of **11h** and **11i** were predicted to occupy the binding pocket at which triazine of **11b** was located. Since the binding pocket for phenyl ring of **11b** was narrow (Figure 7B—red circle), it can be inferred that *meta*-substituents on a phenyl ring of triazine derivatives interfered with the binding to the receptor, which explained why **11h** and **11i** were inactive at hA₁ AR.

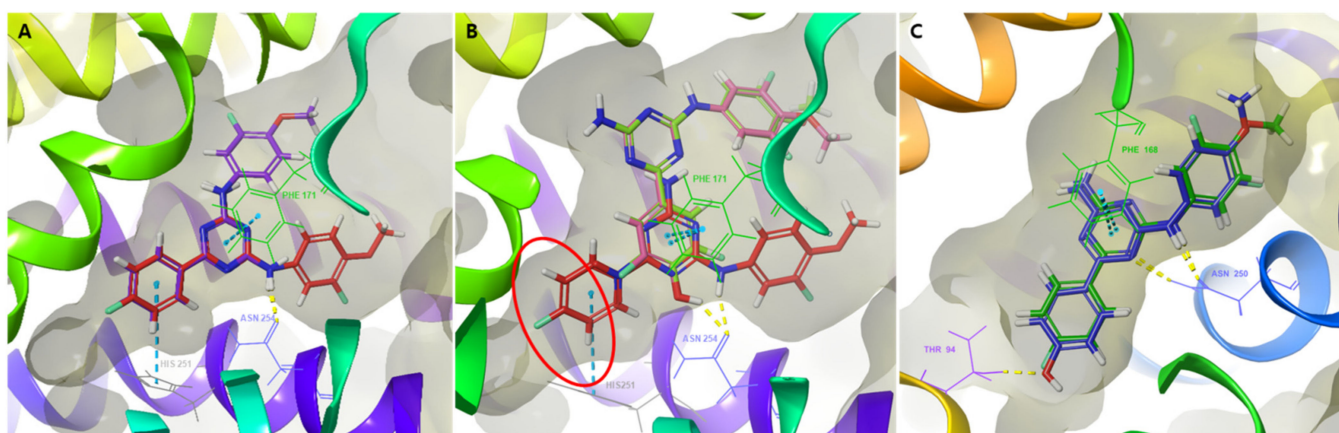


Figure 7. (A) Superimposition of two predicted docking poses in hA₁ AR of **11b**. (B) Superimposition of docking poses in hA₁ AR of **11b** (red carbon atom), **11h** (salmon pink carbon atom), and **11i** (yellow-green carbon atom). The narrow binding pocket for *para*-phenol ring of **11b** is highlighted with a red circle. (C) Superimposition of docking poses in hA₃ AR of **9a** (blue carbon atom) and **11b** (green carbon atom). Hydrogen-bonding and π - π stacking interaction are pictured as yellow and cyan dashed lines, respectively.

We used the previously published homology model of hA₃ AR for docking [27], since the x-ray crystal structure of hA₃ AR has not yet been determined. The ligand used to generate the homology model is structurally distinct from triazine derivatives; therefore, induced-fit docking was utilized to predict the binding mode of **11b** in hA₃ AR. The N250^{6,55} of hA₃ AR generated hydrogen bonds with the nitrogen of aniline and triazine of **11b**, and its triazine formed a π - π interaction with F168^{5,29} (Figure 7C). This was consistent with the binding mode in hA₁ AR, and the docking study explained how **11b** binds to both hA₁ and hA₃ AR. **9a** was predicted to bind in the same manner as **11b** on the hA₃ AR model, which was generated from the **11b** induced-fit docking (Figure 7C).

3. Materials and Methods

3.1. Chemical Synthesis

3.1.1. General Chemical Synthesis

Reagents and solvents were purchased from commercial suppliers (Sigma-Aldrich, Seoul, Korea; Acros Organics, Seoul, Korea; TCI, Seoul, Korea, etc.) and used as provided, unless indicated otherwise. All reactions except Suzuki coupling that used boronic acids with palladium catalysts in a microwave were performed in a round-bottom flask under a nitrogen atmosphere with stirring at room temperature. Reactions were monitored with analytical thin-layer chromatography (TLC) using glass sheets pre-coated with silica gel 60 F₂₅₄ (Merck, Darmstadt, Germany), with visualization under ultraviolet (UV) light (254 nm).

Proton nuclear magnetic resonance ($^1\text{H-NMR}$) spectra of the compounds dissolved in CDCl_3 , deuterated dimethyl sulfoxide ($\text{DMSO-}d_6$), or D_2O , were recorded on a Bruker Avance 400 MHz (Bruker Corporation, Billerica, MA, USA). The chemical shifts were expressed as δ -values in parts per million (ppm) using residual solvent peaks (CDCl_3 : 1H, 7.26 ppm; DMSO : 1H, 2.50 ppm) as a reference. Coupling constants were given in hertz (Hz). The peak patterns are indicated by the following abbreviations: bs = broad singlet, d = doublet, dd = doublet of doublet, m = multiplet, q = quadruplet, s = singlet, and t = triplet. High-resolution spectra were obtained using Waters ACQUITY UPLC[®] BEH C18 1.7 μ -Q-TOF SYNAPT G2-Si (Waters Corporation, Milford, MA, USA) high-resolution mass spectrometry (HRMS). Column chromatography was performed on silica gel 60 (230–400 mesh). Eluent solvents for all chromatographic methods are noted as appropriate mixed solvents with given volume-to-volume ratios.

3.1.2. General Procedure for the Synthesis of **8a–g**

A cyanuric chloride (**7**) solution (1 equiv) in tetrahydrofuran (THF) was stirred and then cooled to $-15\text{ }^\circ\text{C}$. Aniline (1 equiv) was added, and the mixture was stirred at the $-15\text{ }^\circ\text{C}$ for 0.5–1 h. Under TLC monitoring, ammonium hydroxide solution (25–28% NH_3 in water) was added, and the mixture was stirred at room temperature for 1–2 h. Finally, the solvent was removed under reduced pressure, and the resulting solid was collected by filtration and dried to obtain the desired product.

3.1.3. General Procedure for the Synthesis of **9a–g**

Intermediates **8a–g** (1 equiv), (4-hydroxyphenyl)boronic acid (2 equiv), tetrakis (triphenylphosphine)palladium (5 mol%), potassium carbonate (2 equiv), and a 4:1 dioxane:water mixture were added to a microwave tube. The mixture was heated to $120\text{ }^\circ\text{C}$ for 1 h under microwave irradiation and then filtered through Celite with ethyl acetate as an eluent solvent. Next, the filtrate was washed with water and extracted with ethyl acetate. The combined organic layers were washed with brine, dried over anhydrous Na_2SO_4 , filtered, and concentrated in vacuo. Finally, the resulting residue was purified by column chromatography.

Compound **9a**

The 4-{4-amino-6-[(3-fluoro-4-methoxyphenyl)amino]-1,3,5-triazin-2-yl}phenol (**9a**) yield was 62%: $^1\text{H-NMR}$ (400 MHz, $\text{DMSO-}d_6$) δ 9.99 (s, 1H), 9.41 (s, 1H), 8.15 (d, $J = 8.8$ Hz, 2H), 7.87 (d, $J = 12.5$ Hz, 1H), 7.46 (d, $J = 8.2$ Hz, 1H), 7.09 (t, $J = 9.4$ Hz, 1H), 7.00 (s, 2H), 6.85 (d, $J = 8.8$ Hz, 2H), 3.80 (s, 3H); $^{13}\text{C-NMR}$ (100 MHz, $\text{DMSO-}d_6$) δ 170.01, 166.98, 164.32, 160.61, 150.95 (d, $J = 240.5$ Hz); 141.87 (d, $J = 10.9$ Hz); 133.81 (d, $J = 9.8$ Hz); 129.71, 127.48, 115.44, 114.99, 114.02 (d, $J = 2.9$ Hz); 108.22 (d, $J = 22.9$ Hz); 56.26; HRMS (ES⁺): m/z calculated for $\text{C}_{16}\text{H}_{14}\text{FN}_5\text{O}_2$: 328.1210 [M + H]⁺; found 328.1221.

Compound **9b**

The 4-{4-amino-6-[(3,5-dimethoxyphenyl)amino]-1,3,5-triazin-2-yl}phenol (**9b**) yield was 56%: $^1\text{H-NMR}$ (400 MHz, $\text{DMSO-}d_6$) δ 10.02 (s, 1H), 9.33 (s, 1H), 8.17 (d, $J = 8.8$ Hz, 2H), 7.15 (d, $J = 2.3$ Hz, 2H), 7.00 (s, 2H), 6.84 (d, $J = 8.7$ Hz, 2H), 6.14 (t, $J = 2.2$ Hz, 1H), 3.74 (s, 6H); $^{13}\text{C-NMR}$ (100 MHz, $\text{DMSO-}d_6$) δ 170.02, 166.97, 164.55, 160.66, 160.32, 141.84, 129.70, 127.47, 114.99, 98.05, 94.00, 55.02; HRMS (ES⁺): m/z calculated for $\text{C}_{17}\text{H}_{17}\text{N}_5\text{O}_3$: 340.1410 [M + H]⁺; found 340.1436.

Compound **9c**

The 4-{4-amino-6-[(4-chloro-3-methoxyphenyl)amino]-1,3,5-triazin-2-yl}phenol (**9c**) yield was 55%: $^1\text{H-NMR}$ (400 MHz, $\text{DMSO-}d_6$) δ 10.04 (s, 1H), 9.53 (s, 1H), 8.18 (d, $J = 8.8$ Hz, 2H), 7.92 (d, $J = 2.2$ Hz, 1H), 7.44–7.24 (m, 2H), 7.06 (s, 2H), 6.85 (d, $J = 8.8$ Hz, 2H), 3.88 (s, 3H); $^{13}\text{C-NMR}$ (100 MHz, $\text{DMSO-}d_6$) δ 170.13, 166.97, 164.45, 160.71, 154.27, 140.50, 129.78, 129.27,

127.41, 115.04, 113.27, 112.27, 104.51, 55.86; HRMS (ES+): m/z calculated for $C_{16}H_{14}ClN_5O_2$: 344.0914 $[M + H]^+$; found 344.0938.

Compound 9d

The 4-(4-amino-6-[[3-(trifluoromethyl)phenyl]amino]-1,3,5-triazin-2-yl)phenol (**9d**) yield was 82%: 1H -NMR (400 MHz, DMSO- d_6) δ 10.05 (s, 1H), 9.75 (s, 1H), 8.35 (s, 1H), 8.18 (d, $J = 8.9$ Hz, 2H), 8.07 (d, $J = 6.6$ Hz, 1H), 7.52 (t, $J = 7.8$ Hz, 1H), 7.30 (d, $J = 7.6$ Hz, 1H), 7.08 (s, 2H), 6.85 (d, $J = 8.9$ Hz, 2H); ^{13}C -NMR (100 MHz, DMSO- d_6) δ 170.23, 167.07, 164.58, 160.83, 141.08, 130.03–128.68 (m); 129.56, 127.30, 124.38 (q, $J = 272.3$ Hz); 123.08, 117.86, 117.82, 115.83, 115.08; HRMS (ES+): m/z calculated for $C_{16}H_{12}F_3N_5O$: 348.1072 $[M + H]^+$; found 348.1100.

Compound 9e

The 4-(4-amino-6-[[3,5-dimethylphenyl]amino]-1,3,5-triazin-2-yl)phenol (**9e**) yield was 69%: 1H -NMR (400 MHz, DMSO- d_6) δ 9.99 (s, 1H), 9.22 (s, 1H), 8.16 (d, $J = 8.7$ Hz, 2H), 7.46 (s, 2H), 6.93 (s, 2H), 6.84 (d, $J = 8.8$ Hz, 2H), 6.62 (s, 1H), 2.26 (s, 6H); ^{13}C -NMR (100 MHz, DMSO- d_6) δ 170.00, 167.06, 164.57, 160.60, 139.96, 137.24, 129.74, 127.59, 123.47, 117.73, 115.01, 21.28; HRMS (ES+): m/z calculated for $C_{17}H_{17}N_5O$: 308.1511 $[M + H]^+$; found 308.1553.

Compound 9f

The 4-(4-amino-6-[[4-(piperidin-1-yl)phenyl]amino]-1,3,5-triazin-2-yl)phenol (**9f**) yield was 58%: 1H -NMR (400 MHz, DMSO- d_6) δ 9.99 (s, 1H), 9.13 (s, 1H), 8.15 (d, $J = 8.8$ Hz, 2H), 7.60 (d, $J = 9.0$ Hz, 2H), 7.11–6.49 (m, 6H), 3.22–2.86 (m, 4H), 1.79–1.58 (m, 4H), 1.57–1.42 (m, 2H); ^{13}C -NMR (100 MHz, DMSO- d_6) δ 169.87, 167.05, 164.41, 160.49, 147.32, 131.82, 129.70, 127.69, 121.22, 116.33, 114.94, 50.43, 25.44, 23.89; HRMS (ES+): m/z calculated for $C_{20}H_{22}N_6O$: 363.1933 $[M + H]^+$; found 363.1973.

Compound 9g

The 4-(4-amino-6-[[2,4-dimethylphenyl]amino]-1,3,5-triazin-2-yl)phenol (**9g**) yield was 45%: 1H -NMR (400 MHz, DMSO- d_6) δ 9.94 (s, 1H), 8.57 (s, 1H), 8.09 (d, $J = 8.6$ Hz, 2H), 7.27 (d, $J = 7.9$ Hz, 1H), 7.03 (s, 1H), 6.98 (dd, $J = 8.2, 2.3$ Hz, 1H), 6.81 (d, $J = 8.7$ Hz, 2H), 6.75 (s, 2H), 2.27 (s, 3H), 2.18 (s, 3H); ^{13}C -NMR (100 MHz, DMSO- d_6) δ 169.88, 167.25, 165.45, 160.40, 134.67, 133.92, 133.05, 130.70, 129.62, 127.66, 126.36, 114.86, 20.50, 18.06; HRMS (ES+): m/z calculated for $C_{17}H_{17}N_5O$: 308.1511 $[M + H]^+$; found 308.1548.

3.1.4. Procedure for the Synthesis of Intermediate 10

A cyanuric chloride (**7**) solution (1 equiv) in tetrahydrofuran was stirred and then cooled to -15 °C. 3-Fluoro-4-methoxyaniline (1 equiv) was added, and the mixture was stirred at -15 °C for 0.5–1 h. Under TLC monitoring, ammonium hydroxide solution (25–28% NH_3 in water) was added, and the mixture was stirred at room temperature for 1–2 h. Finally, the solvent was removed under reduced pressure, and the resulting solid was collected by infiltration and dried to obtain the desired product.

3.1.5. General Procedure for the Synthesis of 11a–i

Intermediate **10** (1 equiv), R^2 -phenylboronic acid (2 equiv), tetrakis(triphenyl phosphine)palladium (5 mol%), potassium carbonate (2 equiv), and a 4:1 dioxane:water mixture were added to a microwave tube. The mixture was heated to 120 °C for 1 h under microwave irradiation and then filtered through Celite with ethyl acetate as an eluent solvent. Next, the filtrate was washed with water and extracted with ethyl acetate. The combined organic layers were washed with brine, dried over anhydrous Na_2SO_4 , filtered, and concentrated in vacuo. Finally, the resulting residue was purified by column chromatography.

Compound 11a

The *N*²-(3-fluoro-4-methoxyphenyl)-6-(4-methoxyphenyl)-1,3,5-triazine-2,4-diamine (compound **11a**) yield was 76%: ¹H-NMR (400 MHz, CDCl₃) δ 8.33 (d, *J* = 8.9 Hz, 2H), 7.69 (dd, *J* = 13.2, 2.7 Hz, 1H), 7.13 (d, *J* = 8.4 Hz, 1H), 7.03 (s, 1H), 7.01–6.87 (m, 3H), 5.23 (s, 2H), 3.89 (d, *J* = 5.7 Hz, 6H); ¹³C-NMR (100 MHz, DMSO-*d*₆) δ 169.81, 167.02, 164.33, 162.01, 150.96 (d, *J* = 240.5 Hz); 141.94 (d, *J* = 10.9 Hz); 133.73 (d, *J* = 9.8 Hz); 129.54, 129.05, 115.51, 114.01 (d, *J* = 2.9 Hz); 113.66, 108.29 (d, *J* = 22.9 Hz); 56.26, 55.33; HRMS (ES+): *m/z* calculated for C₁₇H₁₆FN₅O₂: 342.1361 [M + H]⁺; found 342.1368.

Compound 11b

The *N*²-(3-fluoro-4-methoxyphenyl)-6-(4-fluorophenyl)-1,3,5-triazine-2,4-diamine (**11b**) yield was 81%: ¹H-NMR (400 MHz, CDCl₃) δ 8.47–8.30 (m, 2H), 7.67 (dd, *J* = 13.2, 2.7 Hz, 1H), 7.21–7.06 (m, 3H), 7.04 (s, 1H), 6.94 (t, *J* = 9.0 Hz, 1H), 5.25 (s, 2H), 3.90 (s, 3H); ¹³C-NMR (100 MHz, DMSO-*d*₆) δ 169.21, 167.06, 164.35, 164.27 (d, *J* = 248.9 Hz); 150.95 (d, *J* = 240.9 Hz); 142.10 (d, *J* = 10.9 Hz); 133.51 (d, *J* = 9.8 Hz); 133.22 (d, *J* = 2.9 Hz); 130.17 (d, *J* = 9.1 Hz); 115.70, 115.31 (d, *J* = 21.4 Hz); 114.00 (d, *J* = 2.9 Hz); 108.44 (d, *J* = 22.9 Hz); 56.25; HRMS (ES+): *m/z* calculated for C₁₆H₁₃F₂N₅O: 328.1010 [M – H][−]; found 328.1013.

Compound 11c

The *N*²-(3-fluoro-4-methoxyphenyl)-6-[4-(trifluoromethoxy)phenyl]-1,3,5-triazine-2,4-diamine (**11c**) yield was 84%: ¹H-NMR (400 MHz, CDCl₃) δ 8.40 (d, *J* = 8.9 Hz, 2H), 7.67 (dd, *J* = 13.2, 2.6 Hz, 1H), 7.30 (d, *J* = 7.9 Hz, 2H), 7.13 (d, *J* = 8.6 Hz, 1H), 7.01 (s, 1H), 6.95 (t, *J* = 9.1 Hz, 1H), 5.25 (s, 2H), 3.90 (s, 3H); ¹³C-NMR (100 MHz, CDCl₃) δ 167.37, 164.89, 152.25 (d, *J* = 244.9 Hz); 152.06, 144.15 (d, *J* = 10.6 Hz); 134.81 (d, *J* = 4.9 Hz); 131.87 (d, *J* = 10.6 Hz); 131.32–118.83 (m); 130.30, 120.51, 116.30 (d, *J* = 3.6 Hz); 113.88 (d, *J* = 2.9 Hz); 110.30, 110.07, 56.82; HRMS (ES+): *m/z* calculated for C₁₇H₁₃F₄N₅O₂: 394.0927 [M – H][−]; found 394.0929.

Compound 11d

The *N*²-(3-fluoro-4-methoxyphenyl)-6-[4-(trifluoromethyl)phenyl]-1,3,5-triazine-2,4-diamine (**11d**) yield was 48%: ¹H-NMR (400 MHz, chloroform-*d*) δ 8.50 (d, *J* = 8.1 Hz, 2H), 7.74 (d, *J* = 8.3 Hz, 2H), 7.66 (dd, *J* = 13.0, 2.5 Hz, 1H), 7.15 (d, *J* = 8.3 Hz, 1H), 6.96 (t, *J* = 9.0 Hz, 1H), 5.47 (s, 2H), 3.91 (s, 3H); ¹³C-NMR (100 MHz, DMSO-*d*₆) δ 168.94, 167.11, 164.35, 150.94 (d, *J* = 241.0 Hz); 142.21 (d, *J* = 11.0 Hz); 140.68, 133.34 (d, *J* = 9.5 Hz); 131.17 (d, *J* = 32.3 Hz); 128.42, 125.36 (d, *J* = 3.9 Hz); 124.15 (d, *J* = 272.2 Hz); 115.78, 114.00 (d, *J* = 2.9 Hz); 108.51 (d, *J* = 22.4 Hz); 56.25; HRMS (ES+): *m/z* calculated for C₁₇H₁₃F₄N₅O: 378.0978 [M – H][−]; found 378.0970.

Compound 11e

The 4-{4-amino-6-[(3-fluoro-4-methoxyphenyl)amino]-1,3,5-triazin-2-yl}benzotrile (**11e**) yield was 85%: ¹H-NMR (400 MHz, DMSO-*d*₆) δ 9.67 (s, 1H), 8.41 (d, *J* = 8.8 Hz, 2H), 8.00 (d, *J* = 8.7 Hz, 2H), 7.88 (s, 1H), 7.44 (d, *J* = 8.8 Hz, 1H), 7.32 (s, 2H), 7.11 (t, *J* = 9.4 Hz, 1H), 3.81 (s, 3H); ¹³C-NMR (100 MHz, DMSO-*d*₆) δ 168.75, 167.08, 164.33, 150.93 (d, *J* = 240.9 Hz); 142.25 (d, *J* = 10.9 Hz); 141.08, 133.25 (d, *J* = 9.8 Hz); 132.46, 128.32, 118.60, 115.83, 113.98 (d, *J* = 2.9 Hz); 113.54, 108.56 (d, *J* = 22.5 Hz); 56.24; HRMS (ES+): *m/z* calculated for C₁₇H₁₃FN₆O: 335.1057 [M – H][−]; found 335.1051.

Compound 11f

The methyl-4-{4-amino-6-[(3-fluoro-4-methoxyphenyl)amino]-1,3,5-triazin-2-yl}benzoate (**11f**) yield was 71%: ¹H-NMR (400 MHz, chloroform-*d*) δ 8.42 (d, *J* = 8.8 Hz, 2H), 8.13 (d, *J* = 8.8 Hz, 2H), 7.68 (dd, *J* = 13.1, 2.6 Hz, 1H), 7.14 (d, *J* = 8.4 Hz, 1H), 7.04 (s, 1H), 6.95 (t, *J* = 9.0 Hz, 1H), 5.27 (s, 2H), 3.95 (s, 3H), 3.90 (s, 3H); ¹³C-NMR (100 MHz, DMSO-*d*₆) δ 169.27, 167.11, 165.91, 164.33, 150.94 (d, *J* = 241.0 Hz); 142.15 (d, *J* = 10.6 Hz); 141.11, 133.40 (d, *J* = 9.5 Hz); 131.87, 129.22, 127.97, 115.71, 114.01 (d, *J* = 2.9 Hz); 108.44

(d, $J = 22.7$ Hz); 56.25, 52.29; HRMS (ES+): m/z calculated for $C_{18}H_{16}FN_5O_3$: 368.1159 $[M - H]^-$; found 368.1145.

Compound 11g

The ethyl-4-[4-amino-6-[(3-fluoro-4-methoxyphenyl)amino]-1,3,5-triazin-2-yl]benzoate (**11g**) yield was 86%: 1H -NMR (400 MHz, chloroform- d) δ 8.41 (d, $J = 8.8$ Hz, 2H), 8.14 (d, $J = 8.8$ Hz, 2H), 7.67 (dd, $J = 13.1, 2.6$ Hz, 1H), 7.15 (d, $J = 8.6$ Hz, 1H), 7.10 (s, 1H), 6.95 (t, $J = 9.0$ Hz, 1H), 5.33 (s, 2H), 4.41 (q, $J = 7.1$ Hz, 2H), 3.90 (s, 3H), 1.42 (t, $J = 7.1$ Hz, 3H); ^{13}C -NMR (100 MHz, DMSO- d_6) δ 169.31, 167.12, 165.43, 164.35, 150.95 (d, $J = 241.2$ Hz); 142.16 (d, $J = 10.9$ Hz); 141.07, 133.42 (d, $J = 9.4$ Hz); 132.16, 129.18, 127.96, 115.73, 114.00 (d, $J = 2.9$ Hz); 108.44 (d, $J = 22.5$ Hz); 60.98, 56.25, 14.17; HRMS (ES+): m/z calculated for $C_{19}H_{18}FN_5O_3$: 384.1466 $[M + H]^+$; found 384.1468.

Compound 11h

The 4-[4-amino-6-[(3-fluoro-4-methoxyphenyl)amino]-1,3,5-triazin-2-yl]-2,6-difluorophenol (**11h**) yield was 68%: 1H -NMR (400 MHz, DMSO- d_6) δ 10.91 (s, 1H), 9.52 (s, 1H), 8.38–7.68 (m, 3H), 7.42 (d, $J = 8.2$ Hz, 1H), 7.29–6.99 (m, 3H), 3.81 (s, 3H); ^{13}C -NMR (100 MHz, DMSO- d_6) δ 168.14, 166.98, 164.23, 151.91 (dd, $J = 241.2, 6.9$ Hz); 150.93 (d, $J = 240.9$ Hz); 142.13 (d, $J = 10.9$ Hz); 136.94 (t, $J = 15.4$ Hz); 133.42 (d, $J = 9.4$ Hz); 127.19 (t, $J = 7.7$ Hz); 115.70, 114.01 (d, $J = 2.9$ Hz); 111.01 (dd, $J = 14.9, 7.6$ Hz); 108.48 (d, $J = 19.6$ Hz); 56.25; HRMS (ES+): m/z calculated for $C_{16}H_{12}F_3N_5O_2$: 362.0865 $[M - H]^-$; found 362.0877.

Compound 11i

The 6-(4-fluoro-3-nitrophenyl)- N^2 -(3-fluoro-4-methoxyphenyl)-1,3,5-triazine-2,4-diamine (**11i**) yield was 66%: 1H -NMR (400 MHz, DMSO- d_6) δ 9.72 (s, 1H), 9.01 (dd, $J = 7.6, 2.0$ Hz, 1H), 8.74–8.52 (m, 1H), 7.91 (s, 1H), 7.76 (dd, $J = 11.2, 8.7$ Hz, 1H), 7.47–7.31 (m, 3H), 7.11 (t, $J = 9.4$ Hz, 1H), 3.81 (s, 3H); ^{13}C -NMR (100 MHz, DMSO- d_6) δ 167.38, 167.04, 164.22, 156.59 (d, $J = 266.3$ Hz); 150.94 (d, $J = 241.2$ Hz); 142.30 (d, $J = 11.3$ Hz); 136.79 (d, $J = 7.6$ Hz); 135.10 (d, $J = 9.8$ Hz); 133.83 (d, $J = 3.6$ Hz); 133.21 (d, $J = 10.2$ Hz); 125.47, 118.96 (d, $J = 21.4$ Hz); 115.82, 113.98 (d, $J = 2.9$ Hz); 108.60 (d, $J = 20.3$ Hz); 56.26; HRMS (ES+): m/z calculated for $C_{16}H_{12}F_2N_6O_3$: 373.0861 $[M - H]^-$; found 373.0866.

3.2. Biological Evaluation

3.2.1. Binding Assay at Human Adenosine Receptors

Binding Assay at hA_1 , hA_{2A} , and hA_3 AR

hA_1 , hA_{2A} , and hA_3 AR competition binding experiments were carried out in a multi-screen GF/C 96-well plate (Millipore, Madrid, Spain) pretreated with binding buffer (Hepes 20 mM, NaCl 100 mM, $MgCl_2$ 10 mM, 2 U/mL adenosine deaminase, pH = 7.4 for hA_1 AR; Tris-HCl 50 mM, EDTA 1 mM, $MgCl_2$ 10 mM, 2 U/mL adenosine deaminase, pH = 7.4 for hA_{2A} AR; and Tris-HCl 50 mM, EDTA 1 mM, $MgCl_2$ 5 mM, 2 U/mL adenosine deaminase, pH = 7.4 for hA_3 AR, respectively). In each well was incubated 5 μ g of membranes from Euroscreen CHO- A_1 cell line, 5 μ g of membranes from Hela- A_{2A} cell line, or 30 μ g of membranes from Hela- A_3 cell line and prepared in laboratory: 1 nM [3H]-DPCPX (140 Ci/mmol, 1 mCi/mL, Perkin Elmer NET974001MC) for hA_1 AR; 1 nM [3H]-ZM241385 (50 Ci/mmol, 1 mCi/mL, ARC-ITISA 0884) for hA_{2A} AR; and 10 nM [3H]-NECA (29.6 Ci/mmol, 1 mCi/mL, Perkin Elmer NET811250UC) for hA_3 AR, respectively; and the compounds studied according to standard protocol. Non-specific binding was determined in the presence of R-PIA 10 μ M (Sigma P4532) for hA_1 AR; of NECA 50 μ M (Sigma E2387) for hA_{2A} AR; and of R-PIA 100 μ M (Sigma P4532) for hA_3 AR, respectively. The reaction mixture (Vt: 200 μ L/well) was incubated at 25 $^\circ$ C for 60 min (hA_1 AR), 30 min (hA_{2A} AR), or 180 min (hA_3 AR); whereafter it was filtered and washed four times (hA_1 and hA_{2A} AR) or six times (hA_3 AR) with 250 μ L wash buffer (Hepes 20 mM, NaCl 100 mM, $MgCl_2$ 10 mM pH = 7.4, for hA_1 AR; Tris-HCl 50 mM, EDTA 1 mM, $MgCl_2$ 10 mM, pH = 7.4, for hA_{2A} AR; and Tris-HCl 50 mM pH = 7.4, for hA_3 AR, respectively) before

being measured in a microplate beta scintillation counter (MicrobetaTrilux, PerkinElmer, Madrid, Spain).

Binding Assay at hA_{2B} AR

hA_{2B} AR competition binding experiments were carried out in a multiscreen GF/C 96-well plate. In each well was incubated 25 µg of membranes from Euroscreen HEK-A_{2B} cell line and prepared in laboratory, 25 nM [³H]-DPCPX (140 Ci/mmol, 1 mCi/mL, Perkin Elmer NET974001MC) and compounds studied according to standard protocol. Non-specific binding was determined in the presence of NECA 1000 µM (Sigma E2397). The reaction mixture (Vt: 250 µL/well) was incubated at 25 °C for 30 min, 200 µL was transferred to GF/C 96-well plate (Millipore, Madrid, Spain), and pretreated with binding buffer (Tris-HCl 50 mM, EDTA 1 mM, MgCl₂ 5 mM, Bacitracin 100 µg/µL, adenosine deaminase 2 U/ML, pH = 6.5). It was then filtered and washed four times with 250 µL wash buffer (Tris-HCl 50 mM, EDTA 1 mM, MgCl₂ 5 mM, pH = 6.5), before being measured in a microplate beta scintillation counter (MicrobetaTrilux, PerkinElmer, Madrid, Spain).

3.2.2. cAMP Accumulation Assay

Antagonist Mode at hA₁ or hA₃ AR

hA₁ and hA₃ AR functional experiments were carried out in CHO-A₁ and CHO-A₃#18 cell line, respectively. The day before the assay, the cells were seeded on the 96-well culture plate (Falcon 353072). The cells were washed with wash buffer (Nutrient Mixture F12 Ham's (Sigma N6658) for hA₁ AR; Dulbecco's modified eagle's medium nutrient mixture F-12 ham (Sigma D8062) for hA₃ AR; 25 mM Hepes; pH = 7.4). Wash buffer was replaced by incubation buffer (Mixture F12 Ham's (Sigma N6658) for hA₁ AR; Dulbecco's modified eagle's medium nutrient mixture F-12 ham (Sigma D8062) for hA₃ AR; 25 mM Hepes, 20 µM Rolipram (Sigma R6520); pH = 7.4). Test compounds and XAC (Sigma X103) or MRS1220 (Sigma M228) as reference compound for hA₁ and hA₃ AR, respectively, were added and incubated at 37 °C for 15 min. Afterward, 0.1 µM of 5'-(*N*-Ethylcarboxamido) adenosine (NECA) (Sigma E2387) was added and incubated at 37 °C for 10 min. FSK (Sigma F3917) was added and incubated at 37 °C for 5 min. After incubation, the amount of cAMP was determined using cAMP Biotrak Enzyme immunoassay (EIA) System Kit (GE Healthcare RPN225).

Agonist Mode at hA₁ or hA₃ AR

hA₁ and hA₃ AR functional experiments were carried out in CHO-A₁ and CHO-A₃#18 cell line, respectively. The day before the assay, the cells were seeded on the 96-well culture plate (Falcon 353072). The cells were washed with wash buffer (Mixture F12 Ham's (Sigma N6658) for hA₁ AR; Dulbecco's modified eagle's medium nutrient mixture F-12 ham (Sigma D8062) for hA₃ AR; 25mM Hepes; pH = 7.4). Wash buffer was replaced by incubation buffer (Mixture F12 Ham's (Sigma N6658) for hA₁ AR; Dulbecco's modified eagle's medium nutrient mixture F-12 ham (Sigma D8062) for hA₃ AR; 25 mM Hepes, 20 µM Rolipram (Sigma R6520); pH = 7.4). The cells were pre-incubated at 37 °C for 15 min. Then, test compounds and 5'-(*N*-Ethylcarboxamido) adenosine (NECA) as reference compound (Sigma E2387) were added and incubated at 37 °C for 10 min. FSK (Sigma F3917) was added and incubated at 37 °C for 5 min. After incubation, the amount of cAMP was determined using cAMP Biotrak Enzyme immunoassay (EIA) System Kit (GE Healthcare RPN225).

3.2.3. Cell Culture

For our study, A549 and NCI-H1299 cells were purchased from the Korean Cell Line Bank (KCLB, Seoul, South Korea). CHO-A₁, Hela-A_{2A}, and HEK-293T-A_{2B} (Euroscreen, Gosselies, Belgium) were also used in this study. The cell culture medium (Roswell Park Memorial Institute (RPMI) 1640, Thermo Fisher Scientific, Waltham, MA, USA) contained 10% fetal bovine serum (FBS) and 1% Antibiotic-Antimycotic (Thermo Fisher Scientific, Waltham, MA, USA) and was used in accordance with guidelines provided by KCLB. The

cells were cultured at 37 °C in an incubator with 5% CO₂. When the cell density reached 90%, subcultures were generated using a trypsin-EDTA solution.

3.2.4. Cell Viability Assay

A549 and NCI-H1299 cells were seeded in 96-well plates at a density of 1×10^5 cells per well for 24 h before being exposed to compounds at various concentrations. After 48 h of compound treatment, the CellTiter 96 AQueous One Solution Cell Proliferation Assay Kit (Promega, Madison, WI, USA) was used to conduct a cell viability assay. The cells were incubated with solution reagents for 2 h at 37 °C before being measured for absorbance at 490 nm using a Synergy HTX Multi-Mode microplate reader (BioTek Instruments, Inc., Winooski, VT, USA).

3.2.5. Microscopy

A549 cells were seeded in 6-well plates at a density of 1×10^6 cells per well for microscopy analysis and then treated with compounds (20 and 40 µM). Cell morphology was examined after 48 h and images of the cells were acquired using an EVOS M5000 Imaging System (Thermo Fisher Scientific Inc., Waltham, MA, USA).

3.2.6. Mitochondrial Membrane Potential (MMP) and Reactive Oxygen Species (ROS) Assay

A549 cells were incubated with a fluorescent indicator, specifically 100 nM tetramethylrhodamine methyl ester perchlorate (TMRM, Thermo Fisher Scientific, Waltham, MA, USA), to determine the mitochondrial membrane potential. The A549 cells treated with the compound were harvested after 48 h, washed in PBS, and re-suspended in FACS buffer (PBS supplemented with 2 percent fetal bovine serum). A flow cytometer (BD FACSVerse, BD Biosciences, San Jose, CA, USA) and the FlowJo software (FlowJo LLC, Ashland, OR, USA) were used to analyze the cells. For the reactive oxygen species measurements, we began by seeding A549 cells in 6-well plates up to a density of 1×10^6 cells in each well, then we treated the cells with the compound (20 and 40 µM) for 48 h. 2',7'-dichlorodihydrofluorescein diacetate acetyl ester (DCFDA) or MitoSOX-red mitochondrial superoxide indicator (Thermo Fisher Scientific, Waltham, MA, USA) was used to detect intracellular and mitochondrial ROS levels. DCFDA (1 µM) or MitoSOX (5 µM) was added to the cells and then incubated at room temperature for 20 min. PBS was then used to wash the cells, and the cells were subsequently re-suspended in FACS buffer (PBS supplemented with 1% FBS). Intracellular fluorescence measurements involved the use of a flow cytometer (BD FACSVerse, BD Biosciences, San Jose, CA, USA) and the FlowJo software (Version 10, TreeStar, Ashland, OR, USA).

3.2.7. Live–Dead Assay

The A549 cells were seeded in 6-well plates at a density of 1×10^6 cells per well, and the cells underwent treatment with the compound (20 and 40 µM) for 48 h. The A549 cells were analyzed using fluorescent dyes for both living and dead cells with the LIVE/DEAD kit (Thermo Fisher Scientific, Waltham, MA, USA). For cell staining, we used EthD-1 and calcein by referring to the manufacturer's instructions. Images were captured with an EVOS M5000 Imaging System (Thermo Fisher Scientific Inc., Waltham, MA, USA).

3.2.8. Statistical Analysis

GraphPad Prism (GraphPad Software, Inc., version 7, San Diego, CA, USA) was used for statistical analysis, and the results were presented as means \pm SEM. The Student's *t*-test was used to further analyze the data. The resulting *p*-values were considered statistically significant (* *p* < 0.05, ** *p* < 0.01, *** *p* < 0.001, **** *p* \leq 0.0001).

3.3. Molecular Modeling

Schrödinger Maestro, version 13.1 (Release 2021-2, Schrödinger, LLC, New York, NY, USA) was used to perform the molecular docking of 1,3,5-triazine derivatives [32].

The structure of 1,3,5-triazine derivatives were drawn using Chemdraw [33] and its 3D conformation was generated using the Schrödinger LigPrep programme [34]. LigPrep generated all possible tautomers and states at pH 7.0 using Epik [35,36] for 1,3,5-triazine derivatives. The crystal structure of hA₁ AR co-crystallized with PSB36 (PDB ID: 5N2S) was acquired from the Protein Data Bank (PDB). The homology model of hA₃ AR was obtained from the research work by Lee et al. [27]. The protein was prepared using the Protein Preparation Wizard [37] to assign bond orders, add hydrogens at pH 7.0, and remove water molecules. Prime was used to complete missing side chains and loops. Finally, a restrained minimization was performed using the default constraint of 0.30 Å RMSD and the OPLS 2005 force field in order to complete the protein preparation. Molecular docking simulations were performed using the Glide ligand docking module for hA₁ AR and the Glide induced fit docking module [38–40] for hA₃ AR in standard protocol (standard precision) mode. The binding conformations of 1,3,5-triazine derivatives were analyzed in order to identify the important interactions with the active site residues of hA₁ and hA₃ AR.

4. Conclusions

We synthesized 1,3,5-triazine derivatives from cyanuric chloride and evaluated their binding affinity toward hARs. Of these derivatives, **11b** showed good binding affinity to both hA₁ and hA₃ AR (K_i = 98.3 and 56.6 nM, respectively; selectivity index = 1.74). **11b** was found to be a hA₁ and hA₃ AR dual antagonist in cAMP accumulation assays at hA₁ and hA₃ AR. Compound **9c** showed the highest binding affinity to hA₁ AR (K_i = 57.9 nM), and we demonstrated that **9c** exhibits cytotoxic activity in lung cancer cells. According to our findings, **9c** increased the expression of ROS, and this accumulation led to mitochondrial membrane dysfunction, which caused cell death. Thus, **9c** is a promising therapeutic agent for lung cancer, and further research efforts should focus on elucidating the mechanisms involved in detail. The binding modes of triazine derivatives were identified through a molecular docking study at hA₁ and hA₃ AR. The 1,3,5-triazine derivatives were predicted to bind to both hA₁ and hA₃ AR. We demonstrated that 1,3,5-triazine derivatives have the potential to be developed as hA₁ and hA₃ AR antagonists. As a result, further SAR efforts on the 1,3,5-triazine derivatives are already underway to improve their efficacy and selectivity to hA₁ or hA₃ AR, or to both hA₁ and hA₃ AR as dual ligands.

Supplementary Materials: The following supporting information can be downloaded at: <https://www.mdpi.com/article/10.3390/molecules27134016/s1>, Figure S1: ¹H and ¹³C NMR Copies of **9a–g** and **11a–i**; Figure S2. HR-MS Copies of **9a–g**, and **11a–i**; Figure S3: Molecular Docking of **9a**, **11b**, **11h** and **11i** in hA₁ AR.

Author Contributions: Conceptualization, J.Y.; data curation, Y.L., S.P. and Y.A.; investigation, H.M.Y., S.P., Y.A., Y.K. and C.H.; methodology, S.P., Y.A. and Y.K.; supervision, H.M.Y., J.Y. and E.J.R.; writing—original draft, H.M.Y., J.Y. and S.P.; writing—review & editing, H.M.Y. and J.Y. All authors have read and agreed to the published version of the manuscript.

Funding: This research was supported by the Ministry of Science and ICT (MSIT), National Research Foundation of Korea (NRF-2022R1C1C1004804 and 2020R1A4A4079494) and the Korea Institute of Science and Technology (KIST) to J.Y. In addition, this work was also supported by the “Establishment of measurement standards for Chemistry and Radiation”, grant number KRISS-2022-GP2022-0003 funded by the Korea Research Institute of Standards and Science and Ministry of Science and ICT (MSIT), National Research Foundation of Korea (NRF-2021M3C1C3097638) to H.M.Y.

Institutional Review Board Statement: Not applicable.

Informed Consent Statement: Not applicable.

Data Availability Statement: All data that generated or analyzed during this study are available from the corresponding authors upon justified request.

Conflicts of Interest: The authors declare no conflict of interest.

Sample Availability: Samples of the compounds are available from the authors.

References

1. Chen, J.F.; Eltzschig, H.K.; Fredholm, B.B. Adenosine receptors as drug targets—What are the challenges? *Nat. Rev. Drug Discov.* **2013**, *12*, 265–286. [[CrossRef](#)] [[PubMed](#)]
2. Saini, A.; Patel, R.; Gaba, S.; Singh, G.; Gupta, G.D.; Monga, V. Adenosine receptor antagonists: Recent advances and therapeutic perspective. *Eur. J. Med. Chem.* **2022**, *227*, 113907. [[CrossRef](#)] [[PubMed](#)]
3. Jacobson, K.; Gao, Z.G. Adenosine receptors as therapeutic targets. *Nat. Rev. Drug Discov.* **2006**, *5*, 247–264. [[CrossRef](#)] [[PubMed](#)]
4. Headrick, J.P.; Peart, J.N.; Reichelt, M.E.; Haseler, L.J. Adenosine and its receptors in the heart: Regulation, retaliation and adaptation. *Biochim. Biophys. Acta* **2011**, *1808*, 1413–1428. [[CrossRef](#)] [[PubMed](#)]
5. Marchi, M.; Raiteri, L.; Risso, F.; Vallarino, A.; Bonfanti, A.; Monopoli, A.; Ongini, E.; Raiteri, M. Effects of adenosine A₁ and A_{2A} receptor activation on the evoked release of glutamate from rat cerebrocortical synaptosomes. *Br. J. Pharmacol.* **2002**, *136*, 434–440. [[CrossRef](#)] [[PubMed](#)]
6. Vannucci, S.J.; Klim, C.M.; Martin, L.F.; LaNoue, K.F. A₁-adenosine receptor-mediated inhibition of adipocyte adenylate cyclase and lipolysis in Zucker rats. *Am. J. Physiol.* **1989**, *257*, E871–E878. [[CrossRef](#)]
7. Gottlieb, S.S. Renal effects of adenosine A₁-receptor antagonists in congestive heart failure. *Drugs* **2001**, *61*, 1387–1393. [[CrossRef](#)] [[PubMed](#)]
8. Kunduri, S.S.; Mustafa, S.J.; Ponnoth, D.S.; Dick, G.M.; Nayeem, M.A. Adenosine A₁ receptors link to smooth muscle contraction via CYP4a, protein kinase C- α , and ERK1/2. *J. Cardiovasc. Pharmacol.* **2013**, *62*, 78–83. [[CrossRef](#)]
9. Gao, Z.G.; Tosh, D.K.; Jain, S.; Yu, J.; Suresh, R.R.; Jacobson, K.A. A₁ adenosine receptor agonists, antagonists, and allosteric modulators. In *The Adenosine Receptors*; Humana Press: Cham, Switzerland, 2018; pp. 59–89.
10. Fishman, P.; Bar-Yehuda, S.; Liang, B.T.; Jacobson, K.A. Pharmacological and therapeutic effects of A₃ adenosine receptor agonists. *Drug Discov. Today* **2012**, *17*, 359–366. [[CrossRef](#)]
11. Borea, P.A.; Gessi, S.; Merighi, S.; Vincenzi, F.; Varani, K. Pharmacology of Adenosine Receptors: The State of the Art. *Physiol. Rev.* **2018**, *98*, 1591–1625. [[CrossRef](#)]
12. Zhou, Y.; Tong, L.; Chu, X.; Deng, F.; Tang, J.; Tang, Y.; Dai, Y. The Adenosine A₁ Receptor Antagonist DPCPX Inhibits Tumor Progression via the ERK/JNK Pathway in Renal Cell Carcinoma. *Cell. Physiol. Biochem.* **2017**, *43*, 733–742. [[CrossRef](#)]
13. Mlejnek, P.; Dolezel, P.; Frydrych, I. Effects of synthetic A₃ adenosine receptor agonists on cell proliferation and viability are receptor independent at micromolar concentrations. *J. Physiol. Biochem.* **2013**, *69*, 405–417. [[CrossRef](#)]
14. Borea, P.A.; Gessi, S.; Bar-Yehuda, S.; Fishman, P. A₃ adenosine receptor: Pharmacology and role in disease. In *Handbook of Experimental Pharmacology*; Springer: Berlin/Heidelberg, Germany, 2009; pp. 297–327.
15. Mazziotta, C.; Rotondo, J.C.; Lanzillotti, C.; Campione, G.; Martini, F.; Tognon, M. Cancer biology and molecular genetics of A₃ adenosine receptor. *Oncogene* **2022**, *41*, 301–308. [[CrossRef](#)]
16. Effendi, W.I.; Nagano, T.; Kobayashi, K.; Nishimura, Y. Focusing on Adenosine Receptors as a Potential Targeted Therapy in Human Diseases. *Cells* **2020**, *9*, 785. [[CrossRef](#)]
17. Gessi, S.; Merighi, S.; Varani, K.; Leung, E.; Lennan, S.M.; Borea, P.A. The A₃ adenosine receptor: An enigmatic player in cell biology. *Pharmacol. Ther.* **2008**, *117*, 123–140. [[CrossRef](#)]
18. Anighoro, A.; Bajorath, J.; Rastelli, G. Polypharmacology: Challenges and Opportunities in Drug Discovery. *J. Med. Chem.* **2014**, *57*, 7874–7887. [[CrossRef](#)]
19. Peters, J.-U. Polypharmacology—Foe or Friend? *J. Med. Chem.* **2013**, *56*, 8955–8971. [[CrossRef](#)]
20. Areias, F.; Correia, C.; Rocha, A.; Brea, J.; Castro, M.; Rosa, M.I.; Proença, M.F.; Carvalho, M.A. 2-Aryladenine derivatives as a potent scaffold for A₁, A₃, and dual A₁/A₃ adenosine receptor antagonists: Synthesis and structure-activity relationships. *Bioorg. Med. Chem.* **2019**, *27*, 3551–3558. [[CrossRef](#)]
21. Abdelrahman, A.; Yerande, S.G.; Namasivayam, V.; Klapschinski, T.A.; Alnouri, M.W.; El-Tayeb, A.; Müller, C.E. Substituted 4-phenylthiazoles: Development of potent and selective A₁, A₃ and dual A₁/A₃ adenosine receptor antagonists. *Eur. J. Med. Chem.* **2020**, *186*, 111879. [[CrossRef](#)]
22. Burbiel, J.C.; Ghattas, W.; Küppers, P.; Köse, M.; Lacher, S.; Herzner, A.-M.; Kombu, R.S.; Akkinepally, R.R.; Hockemeyer, J.; Müller, C.E. 2-Amino[1,2,4]triazolo[1,5-c]quinazolines and derived novel heterocycles: Synthesis and structure-activity relationships of potent adenosine receptor antagonists. *Chem. Med. Chem.* **2016**, *11*, 2272–2286. [[CrossRef](#)]
23. Langmead, C.J.; Andrews, S.P.; Congreve, M.; Errey, J.C.; Hurrell, E.; Marshall, F.H.; Jonathan, S.M.; Richardson, C.M.; Robertson, N.; Zhukov, A.; et al. Identification of Novel Adenosine A_{2A} Receptor Antagonists by Virtual Screening. *J. Med. Chem.* **2012**, *55*, 1904–1909. [[CrossRef](#)]
24. Katritch, V.; Jaakola, V.-P.; Lane, J.R.; Lin, J.; Ijzerman, A.P.; Yeager, M.; Kufareva, I.; Stevens, R.C.; Abagyan, R. Structure-Based Discovery of Novel Chemotypes for Adenosine A_{2A} Receptor Antagonists. *J. Med. Chem.* **2010**, *53*, 1799–1809. [[CrossRef](#)]
25. Masih, A.; Singh, S.; Agnihotri, A.K.; Giri, S.; Shrivastava, J.K.; Pandey, N.; Bhat, H.R.; Singh, U.P. Design and development of 1,3,5-triazine-thiadiazole hybrids as potent adenosine A_{2A} receptor (A_{2A}R) antagonist for benefit in Parkinson's disease. *Neurosci. Lett.* **2020**, *735*, 135222. [[CrossRef](#)]
26. Masih, A.; Agnihotri, A.K.; Srivastava, J.K.; Pandey, N.; Bhat, H.R.; Singh, U.P. Discovery of novel 1,3,5-triazine as adenosine A_{2A} receptor antagonist for benefit in Parkinson's disease. *J. Biochem. Mol. Toxicol.* **2020**, *35*, e22659.

27. Lee, Y.; Hou, X.; Lee, J.H.; Nayak, A.; Alexander, V.; Sharma, P.K.; Chang, H.; Phan, K.; Gao, Z.; Jacobson, K.A.; et al. Subtle Chemical Changes Cross the Boundary between Agonist and Antagonist: New A₃ Adenosine Receptor Homology Models and Structural Network Analysis Can Predict This Boundary. *J. Med. Chem.* **2021**, *64*, 12525–12536. [[CrossRef](#)]
28. Gao, Z.G.; Blaustein, J.B.; Gross, A.S.; Melman, N.; Jacobson, K.A. N⁶-Substituted adenosine derivatives: Selectivity, efficacy, and species differences at A₃ adenosine receptors. *Biochem Pharmacol.* **2003**, *65*, 1675–1684. [[CrossRef](#)]
29. Nogueira, V.; Hay, N. Molecular pathways: Reactive oxygen species homeostasis in cancer cells and implications for cancer therapy. *Clin. Cancer Res.* **2013**, *19*, 4309–4314. [[CrossRef](#)] [[PubMed](#)]
30. Milkovic, L.; Gasparovic, A.C.; Cindric, M.; Mouthuy, P.A.; Zarkovic, N. Short Overview of ROS as Cell Function Regulators and Their Implications in Therapy Concepts. *Cells* **2019**, *8*, 793. [[CrossRef](#)] [[PubMed](#)]
31. Park, J.; Lee, J.; Choi, C. Mitochondrial network determines intracellular ROS dynamics and sensitivity to oxidative stress through switching inter-mitochondrial messengers. *PLoS ONE* **2011**, *6*, e23211. [[CrossRef](#)]
32. *Schrödinger Release 2022-2: Maestro*; Schrödinger, LLC: New York, NY, USA, 2021.
33. Cousins, K.R. Computer Review of ChemDraw Ultra 12.0. *J. Am. Chem. Soc.* **2011**, *133*, 8388. [[CrossRef](#)]
34. *Schrödinger Release 2022-2: LigPrep*; Schrödinger, LLC: New York, NY, USA, 2021.
35. Greenwood, J.R.; Calkins, D.; Sullivan, A.P.; Shelley, J.C. Towards the comprehensive, rapid, and accurate prediction of the favorable tautomeric states of drug-like molecules in aqueous solution. *J. Comput. Aided Mol. Des.* **2010**, *24*, 591–604. [[CrossRef](#)]
36. Shelley, J.C.; Cholleti, A.; Frye, L.; Greenwood, J.R.; Timlin, M.R.; Uchimaya, M. Epik: A software program for pKa prediction and protonation state generation for drug-like molecules. *J. Comput. Aid. Mol. Des.* **2007**, *21*, 681–691. [[CrossRef](#)]
37. Sastry, G.M.; Adzhigirey, M.; Day, T.; Annabhimoju, R.; Sherman, W. Protein and ligand preparation: Parameters, protocols, and influence on virtual screening enrichments. *J. Comput. Aid. Mol. Des.* **2013**, *27*, 221–234. [[CrossRef](#)]
38. Friesner, R.A.; Murphy, R.B.; Repasky, M.P.; Frye, L.L.; Greenwood, J.R.; Halgren, T.A.; Sanschagrín, P.C.; Mainz, D.T. Extra Precision Glide: Docking and Scoring Incorporating a Model of Hydrophobic Enclosure for Protein-Ligand Complex-es. *J. Med. Chem.* **2006**, *49*, 6177–6196. [[CrossRef](#)]
39. Halgren, T.A.; Murphy, R.B.; Friesner, R.A.; Beard, H.S.; Frye, L.L.; Pollard, W.T.; Banks, J.L. Glide: A New Approach for Rapid, Accurate Docking and Scoring. 2. Enrichment Factors in Database Screening. *J. Med. Chem.* **2004**, *47*, 1750–1759. [[CrossRef](#)]
40. Friesner, R.A.; Banks, J.L.; Murphy, R.B.; Halgren, T.A.; Klicic, J.J.; Mainz, D.T.; Repasky, M.P.; Knoll, E.H.; Shaw, D.E.; Shelley, M.; et al. Glide: A New Approach for Rapid, Accurate Docking and Scoring. 1. Method and Assessment of Docking Accuracy. *J. Med. Chem.* **2004**, *47*, 1739–1749. [[CrossRef](#)]